Streaming instability in growing cell populations: Supplementary Information

William Mather, Octavio Mondragón-Palomino, Tal Danino,
Jeff Hasty, Lev S. Tsimring

I. EXPERIMENTAL METHODS

Microbial strain and growth conditions

Before each experiment we cultured non-motile strain of bacteria *E. coli* [1] in 50mL LB (10g/L NaCl) with antibiotics (100 μg/ml ampicillin(Amp) and 50 μg/ml kanamycin(Kan)) for approximately 2 hours from an overnight culture. Cells reached an OD_{600} of 0.05-0.1 and were spun down and concentrated in 5mL of fresh media with surfactant concentration of 0.075% Tween20 [Sigma-Aldrich, St.Louis,MO] before loading in a device. During the run cells received the same media(w/ 0.075% Tween20) via diffusion and advection, and grew exponentially filling the trapping regions in a monolayer.

Microscopy and image analysis

Images were acquired using an epifluorescent inverted microscope (TE2000-U, Nikon Instruments Inc.). A plexiglass incubation chamber encompassing the entire microscope was used to maintain the constant ambient temperature 37°C. Phase contrast images were taken at 20x or 60x every 1-2 minutes. Stitching of images and autofocusing were performed by Nikon Elements software. Each image was processed using grayscale morphology techiques in ImageJ [2] and particle-image velocimetry (MatPIV [3]) was used to measure coarse-grained velocity profiles.

II. SUPPLEMENTARY EXPERIMENTAL RESULTS

In addition to Fig. 1d of the main text that showed a space-time diagram for the average escape velocity of cells at the bottom edge of the open trap, here we present a similar plot for the the top part of the open trap, Fig. S1. It demonstrates that the dynamics on both open ends of the traps are qualitatively similar: cells organize in fast streams and slow clusters, which shift laterally as the clusters of large stagnant cells change in size and position.

In order to assess the importance of friction of cells with the wall chambers, we compared cell flows in trap with heights 1.0μm and 1.65μm. These traps are schematized in Fig. S2 a,b where the semi-closed geometry prevents the flow of media from sweeping cells away, allowing trap height to be larger than 1.0μm. The spatial distribution of vertical velocities in the 1.0μm case is shown in Fig. S2c and the corresponding space-time diagram of exit velocities is shown in Fig. S2 d. One stream is clearly identified at the middle of the trap with transient shifts in location and magnitude (Supplementary Movie 2). A snapshot of the cell flow in the $\sim$1.65μm trap is shown in Fig. S2e and the space-time diagram shown in Fig. S2f. Here, cells are pushed out in a nearly uniform flow across the entire trap, and no streaming pattern is observed.

To study the effect of cell size distribution on streaming, we grew a colony of *E. coli* in a 300x90x0.95 μm^3 open trap, which allows for better distribution of nutrients and more homogenous cell sizes throughout the trap (Fig. S3, Supplementary Movie 4). Because the trap is smaller, cells do not have time to grow large enough and form clusters near the periphery. Thus, cells leave the colony uniformly on both open boundaries of the trap. Interestingly, the PIV analysis of the experiment shows that the magnitude of the exit velocity on either side of the trap is anti-correlated (see the space-time plots in Figs. S3 b and c), which corresponds to the asymmetric regime of cell flow predicted by the continuum theory (see Sec. IV).

Fig. S4 illustrates the cell size dependence on the position within the side trap. In Panel **a** we show a snapshot of the side trap where the cells in the interior are significantly smaller than ones near the exit. Panel **b** shows the average cell area as a function of distance from the open side of the trap. As can be observed in this plot, cell area changes by a factor of 2 from the nutrient-rich open edge of the trap to the back wall. The cross section area of cells was measured by dividing the trap in five horizontal sections centered at z = 9, 27, 45, 63, and 81 μm and segmenting images of cells with ImageJ.

III. DEPTH OF NUTRIENT DEPLETION IN MICROFLUIDIC TRAPS

Our experimental data on the cell size dependence on the distance from the open boundaries (previous Section) suggest that there is variability in the environmental conditions across the trap. The most obvious candidate for such variability is the media which diffuses into the trap from the open boundary and is consumed by growing cells. Here we estimate the characteristic depth z_d of the region near the open boundaries to which the nutrient can penetrate before it is being completely consumed by bacteria, and show that it is in a good agreement with the observed depth of the region in the microfluidic traps where large, healthy cells can be found. Derivation of this estimate uses a connection between the distribution of cells in a microfluidic trap and the growth of cells in a batch culture which has been previously studied in the literature [4].

There are several assumptions used in the analysis, but we do not believe these assumptions strongly affect our estimate. We assume that there exists a single preferred nutrient source (at concentration c which in general is a function of space and time) in the media (Luria-Bertani broth), and that fresh media contains this nutrient at a concentration c_0. Cells are labeled "healthy" when $c > 0$ locally, while cells are "stressed" when $c \approx 0$ locally. The temporal transition between healthy and stressed cells in batch culture appears as a sudden reduction in the apparent mass per cell [4]. We further assume that the consumption rate μ of the nutrient and the doubling time τ do not depend on the local

concentration of the nutrient, although this assumption can be relaxed for more accurate estimates.

A. Depletion of nutrient in a well-stirred batch culture

We now show that the nutrient consumption rate μ can be estimated by analyzing the growth of cells in batch culture. The resulting expression for μ will be used in the next subsection.

Define $n(t)$ as the concentration of cells at time t, and define $c(t)$ as the limiting nutrient concentration at time t. Growth of the cells is exponential

$$n(t) = n_0\, 2^{\,t/\tau} \tag{1}$$

The nutrient concentration is depleted by the cells at a rate μ

$$\frac{dc}{dt} = -n(t)\,\mu = -n_0\,\mu\, 2^{\,t/\tau} \quad , \quad c(t) > 0 \tag{2}$$

Eq. 2 can be integrated to find to the solution for $c(t)$

$$c(t) = c_0 + \frac{\tau\, n_0\, \mu}{\ln 2}\left(1 - 2^{\,t/\tau}\right) = c_0 + \frac{\tau\,\mu}{\ln 2}\left(n_0 - n(t)\right) \tag{3}$$

where $c_0 \equiv c(0)$. Depletion of the nutrient occurs at time t_d, such that $c(t_d) = 0$. By Eq. 3,

$$n(t_d) = \frac{\ln 2\, c_0}{\tau\mu} + n_0 \tag{4}$$

We assume that we work in the limit of a small inoculum, i.e. $n_0 \approx 0$. Then

$$n(t_d) = \frac{\ln 2\, c_0}{\tau\mu} \tag{5}$$

Define $n_d \equiv n(t_d)$. Then, we can express μ in terms of n_d, c_0, and τ:

$$\mu = \frac{\ln 2\, c_0}{\tau\, n_d} \tag{6}$$

Experimentally, n_d is indicated by a sudden change in the apparent mass per cell [4].

B. Distribution of nutrient in a trap

We now model distribution of the nutrient in a microfluidic trap in contact with the fresh media at fixed concentration c_0 along the open boundary at $z = 0$. We assume that cells are present at a constant density n within the trap. We assume a reaction-diffusion model for the nutrient

$$\frac{\partial c}{\partial t} = D\frac{\partial^2 c}{\partial z^2} - n\,\mu \quad , \quad c(z) > 0 \tag{7}$$

where z is a depth coordinate for the trap, and D is the effective diffusion constant for the nutrient. Steady state of this system implies

$$\frac{\partial^2 c}{\partial z^2} = \frac{n\,\mu}{D} \tag{8}$$

which has the solution

$$c(z) = \left(\frac{n\,\mu}{2D}\right)\, z^2 + C_1 z + c_0 \tag{9}$$

with C_1 a constant to be determined. For a sufficiently deep trap, $c(z)$ will become zero at some critical value $z = z_d$. At this point, both $c(z_d)$ and the diffusive flux $-D\frac{\partial c}{\partial z}(z_d)$ are zero, i.e.

$$\frac{\partial c}{\partial z}(z_d) \;=\; 0 = \left(\frac{n\,\mu}{D}\right)\, z_d + C_1 \tag{10}$$

$$c(z_d) \;=\; 0 = \left(\frac{n\,\mu}{2D}\right)\, z_d^2 + C_1 z_d + c_0 \tag{11}$$

Eq. 10 can be used to find C_1, such that

$$c(z) = \left(\frac{n\,\mu}{2D}\right)\, z^2 - \left(\frac{n\,\mu}{D}\right)\, z_d\, z + c_0 \tag{12}$$

Furthermore, Eq. 11 implies

$$c(z_d) = 0 = \left(\frac{n\,\mu}{2D}\right)\, z_d^2 - \left(\frac{n\,\mu}{D}\right)\, z_d^2 + c_0 = -\left(\frac{n\,\mu}{2D}\right)\, z_d^2 + c_0 \tag{13}$$

which leads to the expression for the depth of healthy cells

$$z_d = \sqrt{\frac{2D\,c_0}{n\,\mu}} \tag{14}$$

Using the batch result Eq. 6 for μ, Eq. 14 can be rewritten as

$$z_d = \sqrt{\frac{2D\,\tau}{\ln 2}\,\frac{n_d}{n}} \tag{15}$$

which is independent of c_0.

In order to estimate for the value of the depletion depth, z_d, we obtained parameter values from the literature:

- $n_d = 8.3 \times 10^{-14}\,M$, corresponding to 5×10^7 cells per mL when OD600=0.3 [4].
- $n = 5.5 \times 10^{-10}\,M$, approximating the close packing of cells with cell volume $\sim 3\ \mu\mathrm{m}^3$.
- $D = 880\,\mu\mathrm{m}^2/s$, the diffusion constant reported for serine, a representative amino acid, in water at $25°C$ [5]. This is consistent with the suggestion that the limiting nutrient is an amino acid [4].
- $\tau = 20$ min $= 1200\,\mathrm{s}$, often reported as the doubling time for E. coli [4].

Using the above quantities, we find $z_d \approx 21\ \mu$m. However the estimate can be revised by noticing that diffusion should be faster in our experiments, which occur at a higher temperature ($37°C$). Supposing that D scales with respect to temperature and viscosity according to the Stokes formula for the diffusion constant of a sphere, we revise our estimate to be $z_d \approx 25\ \mu$m.

IV. NARROW CHANNEL FLOW - POLYNOMIAL EXPANSION

The equations of motion for the narrow channel flow (4)-(6) from the Main text can be further reduced in the case that $f(z,t)$ and $c(z)$ are polynomials in z. Suppose

$$\begin{aligned} f(z,t) &= \sum_{n=0}^{N} f_n(t)\, z^n \\ c(z,t) &= \sum_{n=0}^{N} c_n\, z^n \end{aligned} \tag{16}$$

where many c_n may be zero (e.g. $c_n = 0$ for $n > 4$). Then Eqs. (4)-(6) of the Main text lead to

$$\sum_{n=0}^{N} \frac{df_n}{dt}\, z^n + (\alpha z + v_0(t)) \sum_{n=0}^{N} f_n\, n\, z^{n-1} \;=\; \gamma \sum_{n=0}^{N} (c_n - f_n)\, z^n \tag{17}$$

By identifying corresponding coefficients, we finally arrive at the set of ODEs

$$\frac{df_n}{dt} \;=\; -n\alpha f_n - (n+1) v_0(t) f_{n+1} + \gamma(c_n - f_n) \quad ,\ 0 \le n < N \tag{18}$$

$$\frac{df_N}{dt} \;=\; -N\alpha f_N + \gamma(c_N - f_N) \tag{19}$$

Equations (18)-(19) provide a closed set of ODEs for narrow channel flow which was used for the numerical bifurcation analysis shown in the Main Text.

Notice that high order coefficients of f remain zero if initially zero. That is, if $c_n = 0$ and $f_n(t = 0) = 0$ for $M \leq n \leq N$, then $f_n(t) = 0$ for $M \leq n \leq N$.

For the side trap geometry ($v_0 = 0$), all f_n decouple from one another. Equations (18) and (19) can then be used to show that symmetric flow is globally stable.

V. LINEARIZED EQUATIONS FOR SMALL PERTURBATIONS ABOUT ZEROTH-ORDER SOLUTION IN A SIDE TRAP

Streaming is simplest to analyze in the case where narrow channel-like asymmetric instabilities are forbidden by geometric constraints. This can be done by analyzing a side trap, where instead of two open walls at $z = \pm L_z$, there is an open wall at $z = L_z$ and a solid wall at $z = 0$. In the following, we present a brief derivation of the equations governing eigenfunctions in a side trap geometry. These equations can be investigated with a mathematical analysis package capable of solving boundary value problems. We do this using the program Maple (version 11). Solutions are first extended from $z = 0$ to $z = \epsilon$ by a high order, but approximate, polynomial solution, in order to avoid singular behavior of the solution near the solid wall. Maple solves the boundary value problem with this polynomial-extended boundary condition.

A. $\mu = 0$ linearized equations

First consider the case of negligible granular viscosity, i.e. $\mu = 0$. We assume that the zeroth-order solutions, $v_0(z)$ and $f_0(z)$, are perturbed by the functions

$$\tilde{v}_z(x,z,t) = e^{\lambda t}\, e^{ikx}\, v(z) \tag{20}$$

$$\tilde{v}_x(x,z,t) = \frac{i}{k}\, e^{\lambda t}\, e^{ikx}\, \frac{\partial v}{\partial z}(z) \tag{21}$$

$$\tilde{p}(x,z,t) = e^{\lambda t}\, e^{ikx}\, p(z) \tag{22}$$

$$\tilde{f}(x,z,t) = e^{\lambda t}\, e^{ikx}\, f(z) \tag{23}$$

Note that $\partial\tilde{v}_x/\partial x + \partial\tilde{v}_z/\partial z = 0$, such that the full divergence $\vec{\nabla}\cdot(\vec{v}_0 + \vec{\tilde{v}}) = \alpha$. The linearized equations that govern the growth of perturbations are straightforward to derive, with the result

$$g(f_0)\frac{\partial v}{\partial z} + k^2 p = 0 \tag{24}$$

$$\frac{\partial p}{\partial z} + g'(f_0)\, f v_0 + g(f_0) v = 0 \tag{25}$$

$$v_0\frac{\partial f}{\partial z} + (\gamma + \lambda) f + v\frac{\partial f_0}{\partial z} = 0 \tag{26}$$

where $g'(f) = dg(f)/df$. Equations 24-26 must satisfy the boundary conditions

$$v(0) = 0 \tag{27}$$

$$f(0) = 0 \ , \ (\lambda \neq -\gamma) \tag{28}$$

$$p(L) = 0 \tag{29}$$

The boundary condition in Eq. (28) follows from Eq. (26) if $\lambda \neq -\gamma$, since it can be expected that $v_0(\partial f/\partial z) + v(\partial f_0/\partial z) = 0$ at $z = 0$. $f(0)$ may be nonzero if $\lambda = -\gamma$ exactly, but because these eigenfunctions are always stable, they are not relevant to cell streaming.

Eigenfunctions for the side trap geometry can be associated with the eigenfunctions for

the open trap geometry with symmetric uniform flow as the zeroth order approximation. The boundary conditions are then $p(\pm L_z) = 0$ and $f(0) = 0$ (when $\lambda \neq -\gamma$). Symmetry of the open trap eigenfunctions satisfying Eqs. (24)-(26) is chosen such that v_0 and f_0 are odd and even, respectively, with respect to z. This choice ensures that $v(0) = 0$, as is necessary for a side trap.

1. $\mu = 0$ lowest order solutions for $k \to 0$

Instead of $v(z)$, consider the scaled function $w(z) = v(z)/k^2$. The boundary condition for $w(z)$ is $w(0) = 0$. Then Eqs. (24)-(26) can be rewritten

$$g(f_0)\frac{\partial w}{\partial z} + p \;=\; 0 \tag{30}$$

$$\frac{\partial p}{\partial z} + g'(f_0)\, f v_0 + k^2\, g(f_0) w \;=\; 0 \tag{31}$$

$$v_0\frac{\partial f}{\partial z} + (\gamma + \lambda) f + k^2\, w\frac{\partial f_0}{\partial z} \;=\; 0 \tag{32}$$

In lowest order in k^2 (assuming w is order 1) these equations are

$$g(f_0)\frac{\partial w}{\partial z} + p \;=\; 0 \tag{33}$$

$$\frac{\partial p}{\partial z} + g'(f_0)\, f v_0 \;\approx\; 0 \tag{34}$$

$$v_0\frac{\partial f}{\partial z} + (\gamma + \lambda) f \;\approx\; 0 \tag{35}$$

Analytic solutions for the $k = 0$ case can be indexed by a nonnegative integer m, such that

$$\lambda_m \approx -(\gamma + m\alpha) \tag{36}$$

$$f_m(z) \approx z^m \tag{37}$$

$$p_m(z) \approx \alpha \int_z^L dz_1 \; g'(f_0(z_1)) \; z_1^{m+1} \tag{38}$$

$$w(z) \approx -\int_0^z dz_1 \frac{p(z_1)}{g(f_0(z_1))} \tag{39}$$

B. Linearized equations for non-zero viscosity

The condition $\mu = 0$ is somewhat unrealistic for a granular flow. While $\mu \neq 0$ effects do not appear for narrow channel flow, we find that stability of uniform flow is significantly increased by a small value for μ.

Linearization of the dynamics for $\mu \neq 0$ can be done as in the $\mu = 0$ case. The equations analogous to Eqs. (30)-(31) are now

$$g(f_0)\frac{\partial v}{\partial z} + k^2 p - \mu \frac{\partial}{\partial z}\left(\frac{\partial^2 v}{\partial z^2} - k^2 v\right) = 0 \tag{40}$$

$$\frac{\partial p}{\partial z} + g(f_0)v + g'(f_0)\, f\, v_0 - \mu\left(\frac{\partial^2 v}{\partial z^2} - k^2 v\right) = 0 \tag{41}$$

The boundary conditions in Eqs. (27)-(29) continue to apply. Additionally, we assume a continuous tangential stress condition (a slip condition) at both the inner wall and the outer free boundary, which can be written in this case as

$$\frac{\partial \tilde{v}_x}{\partial z} + \frac{\partial \tilde{v}_z}{\partial x} = 0 \tag{42}$$

For the velocity function $v(z)$, this condition leads to boundary conditions

$$k^2 v(0) + \frac{\partial^2 v}{\partial z^2}(0) \;=\; 0 \tag{43}$$

$$k^2 v(L) + \frac{\partial^2 v}{\partial z^2}(L) \;=\; 0 \tag{44}$$

Calculations reported in the main text solve these equations using solutions that are odd in v.

VI. DISCRETE ELEMENT SIMULATIONS

A. Details of simulation algorithm

Our basic algorithm for soft-particle simulations of growing and dividing spherocylinders has been described previously [6]. It calculates normal and tangential forces between cells based on the overlap of virtual soft spheres centered at the nearest points on the axes of interacting spherocylinders. The motion of the cylinders is obtained by the integrating the Newton's equations using 4th order predictor-corrector scheme, and each cell's length ℓ and f-factor are governed by the first-order ODEs associated with each cell. After the cell length exceeds a certain prescribed value ℓ_{div}, the cell is replaced by two collinear cells with half its length at the same location.

Cells experience negligible sliding friction from motion against the solid side walls of the trap (defining the x and z boundaries) or against other cells. The time step is $\sim 0.25 \times 10^{-5}$ (AU). The average length of division ℓ_{div} is typically short, i.e. $\ell_{div} = 3$, but $\ell_{div} = 5$ is used for the simulations mentioned in Section VI B. The actual division length is chosen randomly from a Gaussian distribution with mean ℓ_{div} and coefficient of variation 0.2. Drag force on the cells is proportional to velocity of the cell times the factor $g(f) = 2(f/d)^2\mathrm{M}$, with $\mathrm{M} = 1 + 1.5(\ell - d)$ the dimensionless mass of the cell, and ℓ the current length of the cell. Most of the other parameters in the simulation are the same

as in Ref. [6].

In Fig. 6 we show an example of DES simulation of a periodic cell flow in a narrow open channel, and compare it with analytical theory discussed in the main text.

B. The role of cell shape in streaming

Though cell streaming can be theoretically investigated without including the effects of cell shape, simulations suggest that colonies of longer cells are more prone to destabilize into streams. Additionally, streams of long cells tend to be more highly focused. Fig. S7a presents space-time diagrams demonstrating streaming of long cells, with a snapshot of the cell configuration appearing in Fig. S8a. Figures S7b, c and S8b, c show the dynamics of short cells for comparison. The full time-lapse movie of the corresponding simulation runs are shown in Supplementary Movies 6 and 7. We conjecture that long rods enhance streaming by (i) reducing granular viscosity by local ordering of cells into flowing layers, and (ii) orienting the stress tensor along the direction of streams.

[1] J. Stricker, S. Cookson, M. R. Bennett, W. H. Mather, L. S. Tsimring, and J. Hasty, Nature **456**, 516 (2008).

[2] http://rsbweb.nih.gov/ij/.

[3] J. K. Sveen, *An introduction to MatPIV v.1.6.1*, Eprint no. 2, **ISSN** 0809-4403, Dept. of Mathematics, University of Oslo (2004), http://www.math.uio.no/~jks/matpiv.

[4] G. Sezonov, D. Joseleau-Petit, and R. D'Ari, J. Bacteriol. **189**, 8746 (2007).

[5] P. S. Stewart, Journal Of Bacteriology **185**, 1485 (2003).

[6] D. Volfson, S. Cookson, J. Hasty, and L. S. Tsimring, Proc. Natl. Acad. Sci. USA **105**, 15346 (2008).

[7] A. Dhooge, W. Govaerts, and Y. A. Kuznetsov, ACM T. Math. Software **29**, 141 (2003).

[8] J. Guckenheimer and P. Holmes, *Nonlinear Oscillations, Dynamical Systems, and Bifurcations of Vector Fields* (Springer-Verlag, New York, 1983).

List of Supplementary Movies

Movie S1. Time-lapse microscopy of 400 μm-long segment from the 2 mm-long open trap. Images were taken every minute with a 60x objective using phase contrast and stitched together.

Movie S2. Time-lapse microscopy of 90x100x1 μm^3 side trap. Images were taken every minute with a 60x objective using phase contrast.

Movie S3. Time-lapse microscopy of 90x100x1.65 μm^3 side trap. Images were taken every minute with a 60x objective using phase contrast. No streaming is observed in this trap because of the higher depth.

Movie S4. Time-lapse microscopy of 125 μm-long segment from a 90x300x1.65 μm^3 open trap. Images were taken every 2.5 min with a 60x objective using phase contrast.

Movie S5. Numerical simulation of the oscillating flow in a narrow open channel (see Fig. S6 for simulation details)

Movie S6. Numerical simulation of the streaming instability of short cells in a wide side channel (see Fig. S7 for simulation details)

Movie S7. Numerical simulation of the streaming instability of long cells in a wide side channel (see Fig. S7 for simulation details)

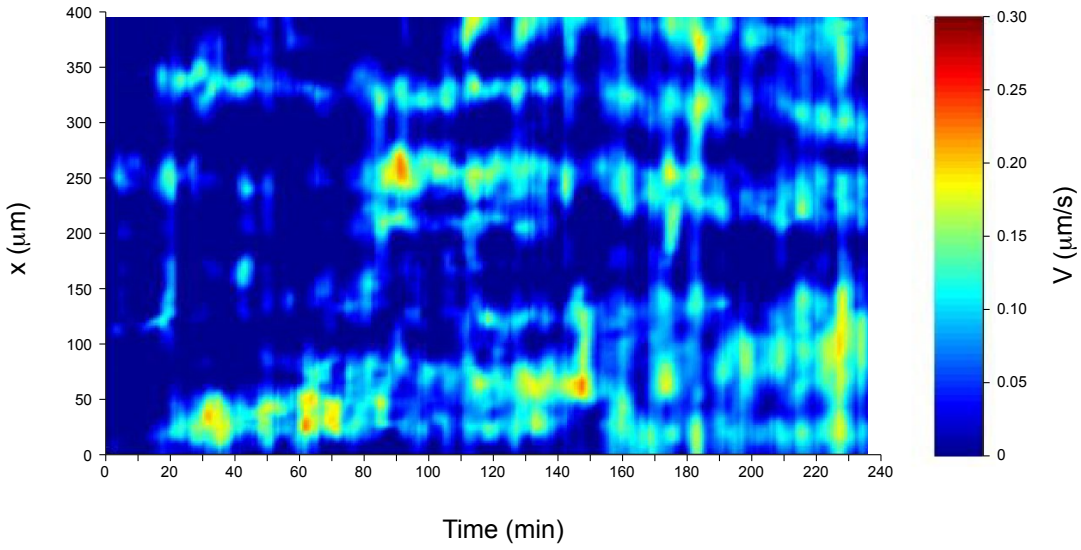

Supplementary Figure S1: Space-time plot of the average exit velocity calculated over $\sim$20 μm near the top edge of the monolayer segment shown in Fig. 1c of the main text.

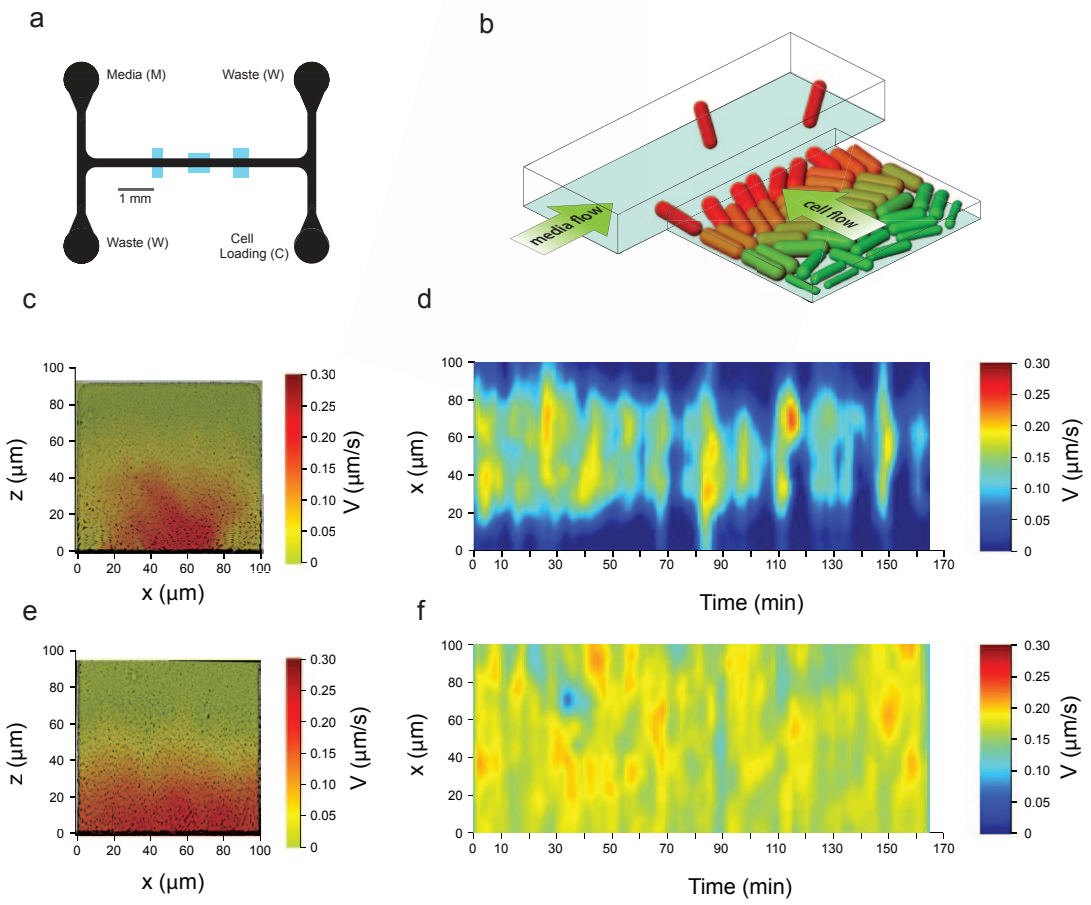

Supplementary Figure S2: **a.** Schematic diagram of the microfluidic device with side traps (light blue rectangles) on either side of the main channel (black). The traps have been magnified 300% for visualization. Traps are seeded with cells from the cell loading port. Cells are supplied with nutrients from the media port, and as they escape from the trap, they are transported by the flow to one of the waste ports. **b.** Sketch of one cell trap. Color indicates the cell "size" **c.** Snapshot of the z-component of velocity overlaid with a phase contrast image of a cell monolayer confined in a 1μm-high side trap. A single "red" stream is flanked by two clusters of large slow moving cells. Deeper in the trap, cells are smaller and almost immobile. This snapshot corresponds to the frame at time 149 minutes in the Supplementary Movie 2. **d.** Space-time plot of the exit velocity calculated over $\sim$20 μm strip at the bottom edge of the monolayer shown in Panel **c**. In this plot, a stream of cells shows up as a horizontal band along the middle. The blue areas around this band represent the flanking slow cells. **e, f.** Plots analogous to **c, d**, but for a 1.65μm-high side trap (see Supplementary Movie 3). In this case, the friction of cells along the wall is reduced to a minimum, and streaming is not pronounced.

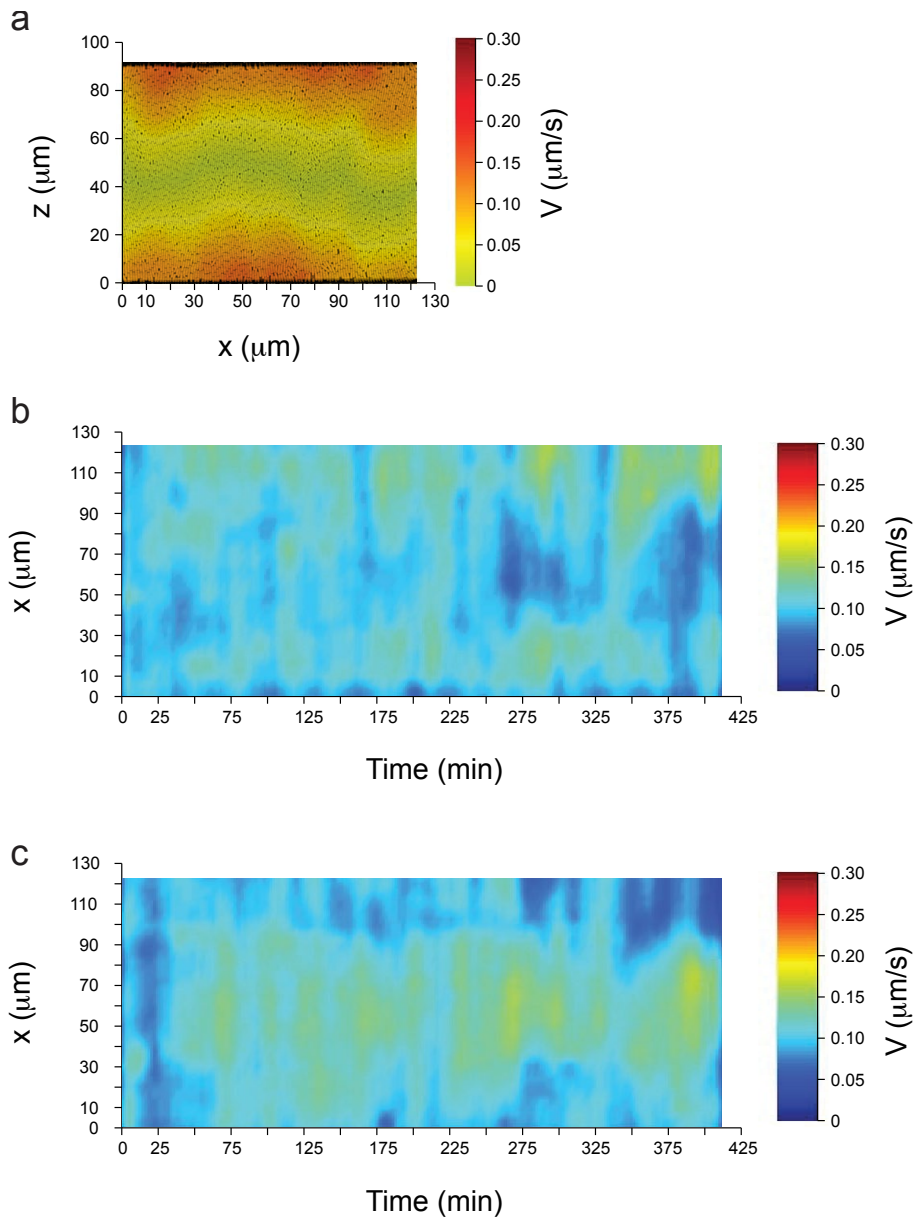

Supplementary Figure S3: a) Magnitude of the vertical component of velocity overlaid with a phase contrast image of a colony in an open trap that is half as wide ($\sim$90μm) as the chamber shown in Fig. 1 of the main text. This snapshot corresponds to time 122.5 min in Supplementary Movie 4. Unlike in other one micron high traps, here cell size seems to be uniform and less affected by any chemical gradients that may exist within the colony, and cells seem to be pushed out without streaming. Space time plots for the average exit velocity at the bottom (b) and top(c) of the trap respectively. The average of velocity was calculated over 20 μm from each edge. These plots show that the escape velocity on both sides of the trap is anticorrelated.

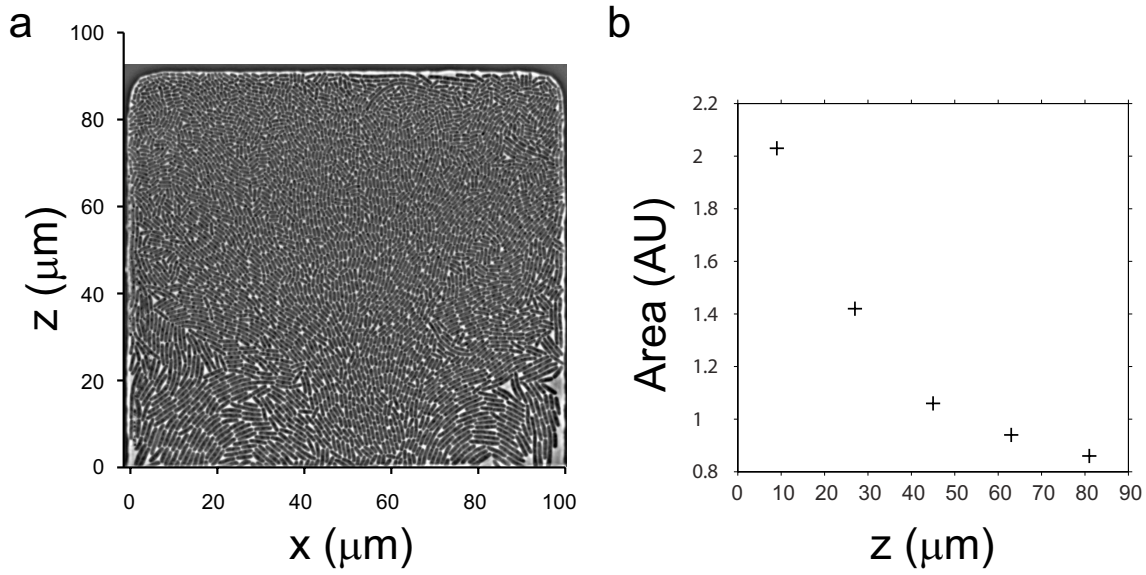

Supplementary Figure S4: **a.** Snapshot of a colony growing in the $\sim 1\mu$m-high chamber described in Fig. S2. **b.** Plot of the average cross sectional area of cells as a function of the distance from the open edge of the trap.

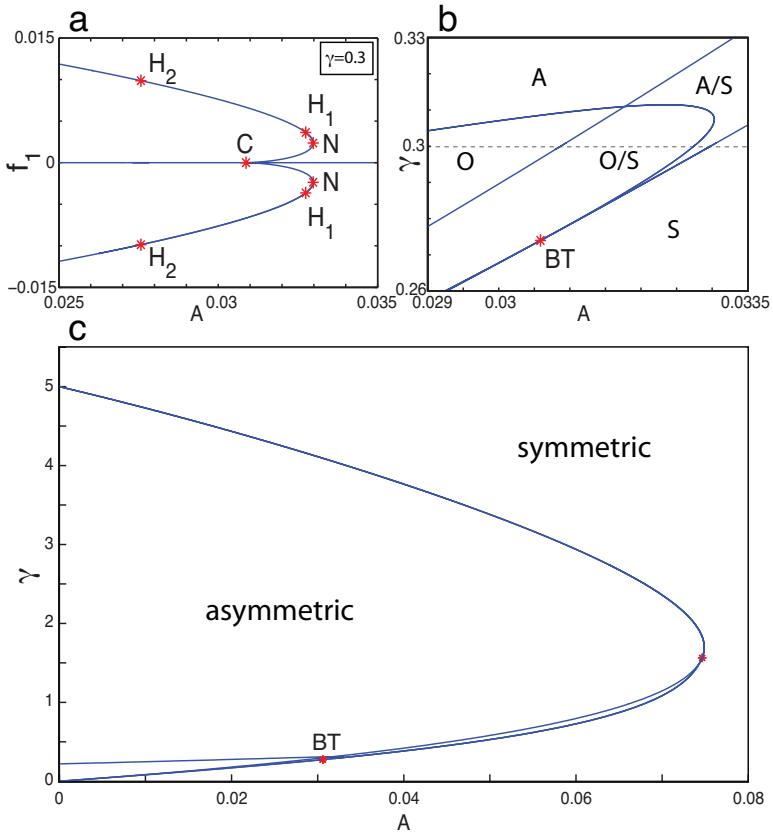

Supplementary Figure S5: A local bifurcation analysis of the narrow channel flow (global bifurcations exist, but are not treated in detail). **a.** One parameter local bifurcation diagram (in coordinates $A \equiv c(0)$ and f_1, the first-order term of the f polynomial). Oscillations appear between Hopf bifurcations H_1 and H_2, while fixed points corresponding to asymmetric solutions exist left of H_2 and between H_1 and the saddle-node point N. Unstable fixed points exist left of C and between C and N. Stable symmetric fixed points ($f_1 = 0$) are right of C. Parameters are $\alpha = 1$, $\gamma = 0.3$, $c(z) = A + (z/L_z)^4$, $g(f) = f^2$, $L_z = 1$. **b.** A two-parameter local bifurcation diagram for the system in **a** in parameters A and γ. Symbols S, A, and O indicate regions with symmetric fixed points, asymmetric fixed points, or oscillations, respectively. Bistable attractors are listed together, e.g. O/S. BT represents a Bogdanov-Takens bifurcation. The dashed line indicates the value of γ used in panel **a**. **c.** A wider view of the bifurcation diagram **b**. The majority of space not belonging to symmetric flow is associated with a pair of asymmetric fixed points. These bifurcation diagrams are derived from local bifurcation analysis in Matcont [7]. Consistent with the appearance of a Bogdanov-Takens bifurcation [8], a global bifurcation analysis is necessary to fully understand the behavior of this system. Numerical investigation confirms the existence of infinite-period homoclinic bifurcations that lead to large-amplitude limit cycles (data not shown).

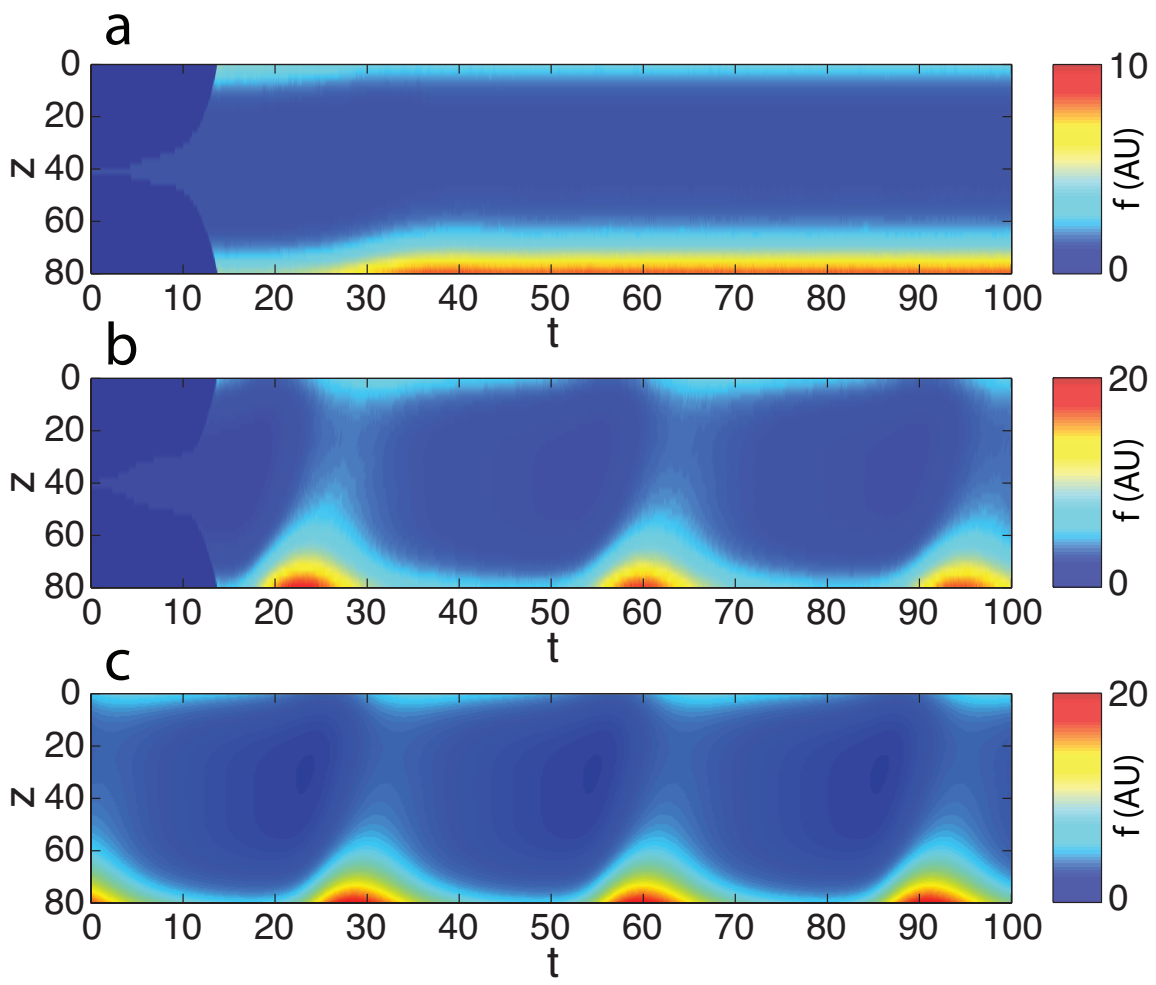

Supplementary Figure S6: Space-time diagrams of the narrow-channel flow. DES simulations were started from a single cell placed in the middle of the trap (narrow width $L_x = 10$, length $2L_z = 80$). Color characterizes the cell "diameter" f averaged within a strip of width 2 along z dimension. **a.** Stationary asymmetric regime is seen for parameters $\gamma = 0.5$, $c(z) = 1 + 20\,(z/L_z)^4$; **b.** Oscillatory behavior is seen for parameters $\gamma = 0.1$, $c(z) = 1 + 100\,(z/L_z)^4$. Both simulations have parameters $\ell_{\rm div} = 3$, $\alpha = 0.5$; **c.** Space-time diagram of f for the continuum description of the narrow-channel flow with the same parameter values.

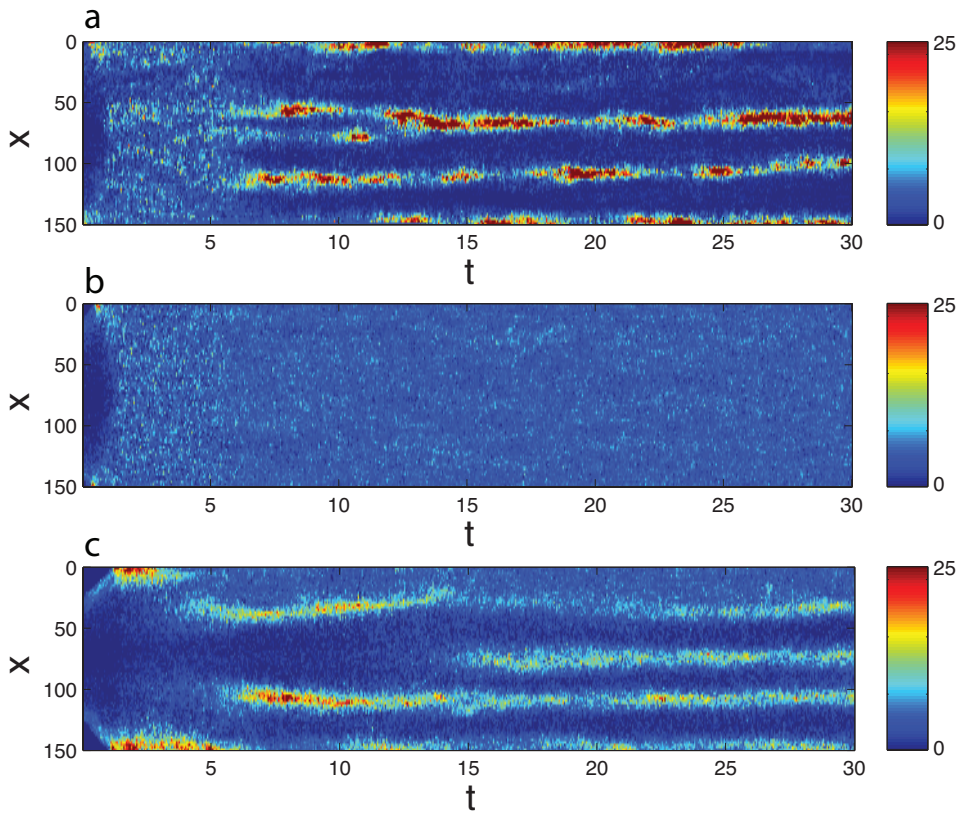

Supplementary Figure S7: Space-time diagrams for simulations of cell flows in wide side traps ($L_x = 150, L_z = 20$) with different cell aspect ratios. **a**. Streaming flow of long cells (average length 5 at division), **b**. Uniform flow of short cells (average length 3 at division), **c.** Short cells with streaming flow. Panels **b** and **c** correspond to the simulations in Fig. 4 of the main text. Other than differing average cell size and elongation rate (the two are balanced to keep the division rate of long cells the same as short cells), the parameters for the simulation in **a** are the same as in **b** and **c**.

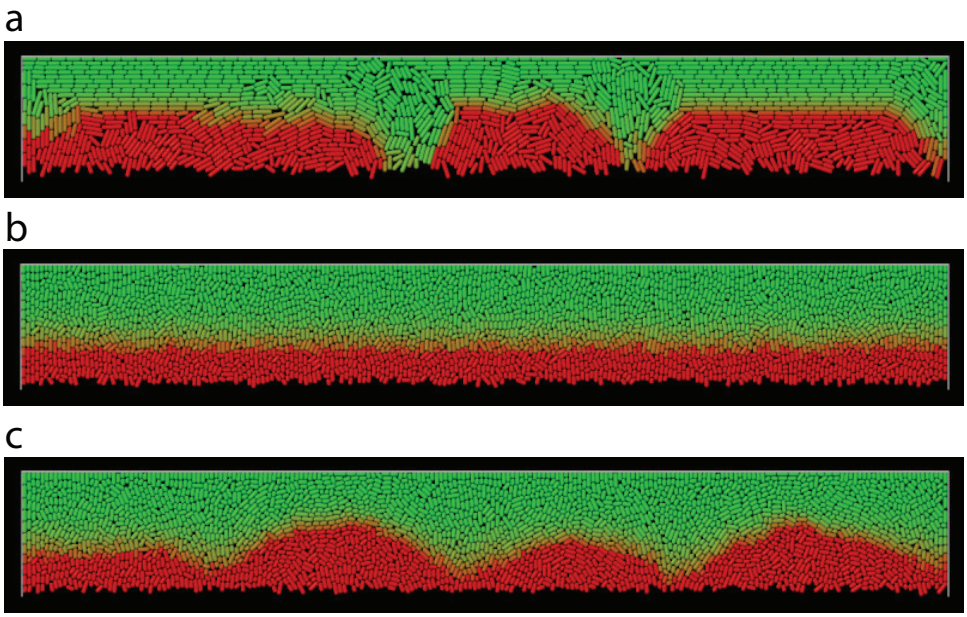

Supplementary Figure S8: Snapshots at time $t = 30$ of the three simulations in Fig. S7. Green and red represent low ($f = 0$) and high ($f \geq 10$) values of f, respectively, for each cell.